Journal of Low Temperature Physics, Vol 71, Nos 5/6, 1988

Design, Optimization, and Construction of a DC SQUID with Complete Flux Transformer Circuits

Jukka Knuutila and Matti Kajola

Low Temperature Laboratory, Helsinki University of Technology, Espoo, Finland

Heikki Seppä

Electrical Engineering Laboratory, Technical Research Centre of Finland, Espoo, Finland

Risto Mutikainen and Jorma Salmi

Semiconductor Laboratory, Technical Research Centre of Finland, Espoo, Finland

(Received November 18, 1987)

The design of a complete dc SQUID with a flux transformer input circuit is discussed. The flux coupling circuits introduce a substantial capacitance across the SQUID and give rise to many resonances which may couple strongly to the SQUID dynamics. Both effects lead to multiple modes in the SQUID dynamics and consequently to excess noise. For a low-noise SQUID with smooth characteristics, our analysis and practical considerations suggest signal coupling via an intermediary transformer. This method allows simultaneous optimization of the SQUID parameters, minimizing the parasitic capacitance, control over the resonances, and good inductance matching to practical magnetometer coils. A model is developed to optimize the structure: it describes the whole circuit with the help of a suitably modified autonomous SQUID, provided that the system is free from multiple modes due to resonances or large parasitic capacitance. Following these design principles, we have built a dc SQUID, primarily for use in biomagnetic research, but also well suited for other applications. The fabrication of the SQUID and the high-quality electronics especially suitable for multiple-SQUID devices is presented. The SQUIDs showed smooth characteristics, and the lowest measured noise of our complete SQUID is $1.3 \times 10^{-6} \Phi_0/\sqrt{Hz}$, indicating the success of the design.

1. INTRODUCTION

During the last few years, high-sensitivity dc SQUIDs with tightly coupled input coils have been introduced.[1-7] However, the flux transformer circuits of practical magnetometers affect the SQUID dynamics markedly because of the parasitic elements inevitably present in thin-film circuits.

0022-2291/88/0600-0369$06.00/0

Several magnetometers have been produced without paying special attention to these unwanted features. The parasitic capacitance gives rise to hysteresis in the current-voltage characteristics and multiple modes in the SQUID dynamics, accompanied by excess noise.

Although the extra capacitance across the SQUID loop introduced by the input coil has been studied by several authors with simulations[8-12] and experiments,[13-16] no systematic design approach on that basis has been given. Some interesting approaches to eliminate the parasitic elements, however, have been suggested. In the double-loop SQUID construction of Tesche discussed in Refs. 8 and 2, the parasitic capacitance is in parallel with a capacitance used to separate the SQUID loop into two parts. Since the extra resonance introduced by the capacitances was not separately damped, the noise invoked by the multiple modes tended to increase the noise level specifically at low bias currents.[17] The problem was treated completely differently by Enpuku *et al.*[10,18-20] In their approach, both the loop inductance and the stray capacitance were damped by an extra shunt resistor placed across the SQUID ring. The damping was shown to allow the choice of a high loop inductance with only a slight increase of noise. The noise analysis of this system was made without capacitances, thus ignoring the possibility of excess noise introduced by the multiple modes in the SQUID dynamics. Consequently, the calculations can be used to predict only the noise level of real devices with heavily damped junctions.

In addition to the stray capacitances, the input circuits give rise to many resonances. They lead to excess noise, as was recently predicted by numerical simulations[12] for the signal coil LC resonance. The improvement in the SQUID characteristics and in the noise level obtained by properly damping this resonance has also been experimentally verified.[17]

In SQUIDs suffering from these nonidealities, the noise level as a function of the flux threading the SQUID ring shows very large and sharp changes. Therefore, it may be possible to operate a SQUID in the small-signal mode with carefully chosen flux bias at noise levels comparable to those that can be theoretically obtained with autonomous SQUIDs[21,22] However, any attempts to use a practical configuration with flux modulation and phase-locked loop have resulted in a substantially deteriorated energy resolution.[3,5,15,23]

In this work we discuss the design of a complete low-noise, well-behaving dc SQUID sensor free from most of the problems discussed above. The basis of the whole design is proper damping of all the resonances sensed by the SQUID. On the other hand, one of the most important goals of the design is to make the SQUID dynamics independent of the surroundings. In this way, the SQUID can be used in many applications without the excess noise usually introduced by the coupling circuits. Furthermore,

our design aims at the lowest noise allowed by the fabrication technology. The above general criteria are applied in designing a practical dc SQUID. The sensor is mainly intended for a multichannel, all-planar magnetometer to be used in neuromagnetic research, but it is also well suited for other purposes. Most of the discussion in this paper deals with the design, production, and measurement results of this SQUID magnetometer.

2. GENERAL DESIGN CRITERIA

2.1. Autonomous versus Coupled SQUIDs

The optimization and the design of a dc SQUID magnetometer, with flux coupling circuits ignored, is straightforward. In this case, the choice $\beta = \beta_c = 1$ is regarded as a solid foundation for instrument design. Here $\beta = 2L_s I_0/\Phi_0$ and $\beta_c = 2\pi R^2 I_0 C/\Phi_0$, with L_s being the SQUID loop inductance and I_0, R, and C the junction critical current, shunt resistance, and capacitance, respectively. The intrinsic energy sensitivity of such a device is proportional to $(L_s C)^{1/2}$, suggesting low values both for the inductance L_s and the junction capacitance C. Since the smallest possible junction capacitance is fixed by the available technology, SQUIDs with extremely low loop inductances are needed to reduce the noise. Such miniature devices, however, are not practical in low-noise magnetometers because of difficulties in inductance matching. A large number of turns in the signal coil would be required, and the stray capacitance thereby introduced by the signal coil across the SQUID would partly cancel the advantage of the low junction capacitance by decreasing the damping of the SQUIDs self-resonance.

Sufficiently high output inductance can be achieved without introducing large stray capacitance by using the so called multiloop SQUID.[14] Unfortunately, in this structure the SQUID loop has a tendency to become very long, introducing transmission line resonances which may be close to the Josephson frequencies at the normal points of operation.

The problem related to inductance matching can be solved most conveniently by the use of an intermediate coupling transformer.[5,16] Then, a sufficiently low number of turns can be employed in the input coil, in connection with a small-size SQUID, to reduce the parasitic capacitance across the SQUID.

Practical magnetometers with closely coupled input coils cannot, of course, be optimized using the methods relevant to the design of an autonomous SQUID. However, we have reduced the design of the complete SQUID partly to the design of an autonomous SQUID with the aid of two main ideas, verified by computer simulations:[12,24] (1) the stray capacitance appearing across the SQUID loop should be kept from exceeding the

junction capacitance and (2) any resonances introduced by the signal coil should be properly damped. Otherwise, as our simulations indicate, multiple modes in the SQUID dynamics will appear, leading to increased low-frequency noise. If the above demands are fulfilled, the analysis and computer simulations made for the autonomous SQUID can be used in modeling the SQUID dynamics in the optimization of the coupled SQUID.

2.2. Sensitivity of the Magnetometer

In this section we estimate the ultimate energy sensitivity of the SQUID magnetometer with a flux coupling circuit, which is assumed to be free from the multiple modes and resonances. The analysis is based on the results obtained in simulating well-damped autonomous SQUIDs.[21,22,24] Furthermore, we assume that the length of the signal coil is longer than the wavelength of the Josephson oscillations at the average points of operation. Consequently, the magnetic coupling will be strongly reduced and the inductance of the SQUID loop sensed by the high-frequency dynamics of the SQUID remains independent of the flux coupling circuits. A change of the apparent SQUID inductance toward the unscreened value at high bias currents, and thus at high Josephson frequencies, has also been observed experimentally.[13] Under these circumstances the flux-to-voltage transfer function G can be given approximately as

$$G = \frac{I_0 R}{\Phi_0} \frac{g}{1+\beta} \tag{1}$$

Here, g is a constant whose value, according to computer simulations, is between 1 and 2, depending on the damping of the junctions. It should be emphasized that in Eq. (1) the screening current of the SQUID is ignored; in the more detailed analysis discussed in Section 3.3, its effects are included.

In a SQUID magnetometer with a flux transformer the relevant parameter to be optimized is the energy sensitivity at the input of the flux transforming circuit. The extrinsic energy sensitivity ε_a, i.e., the energy sensitivity in the pickup coil, can be given as a function of the effective flux noise Φ_n in the SQUID input:

$$\varepsilon_a = \frac{\Phi_n^{a2}}{2L_p} = \frac{\Phi_n^2}{2L_s k_s^2 s_f (1-s_f)} \tag{2}$$

Here, the SQUID is assumed to be coupled to the outside world via one flux transformer, with pickup and input coil inductances L_p and L_i, respectively, Φ_n^a is the equivalent flux noise in the pickup coil. The coupling between the SQUID loop L_s and the input coil L_i is k_s. The SQUID inductance is screened at low frequencies by the flux transformer circuit;

the screening factor s_f is given by

$$s_f = \frac{L_i}{L_i + L_p} \tag{3}$$

The noise of the SQUID at frequencies well below the Josephson oscillations is assumed to be solely due to the shunt resistors R of the Josephson junctions, either directly or indirectly. The latter contribution comes via mixing-down processes, resulting from the nonlinearities of the system, or by jumps between the multiple modes of the SQUID dynamics. This effect can be taken into account by multiplying the low-frequency term by a factor γ, which on the basis of numerical simulations has a value of 1.5–2, depending on the junction capacitance C.[22,24] If the junction capacitance is neglected, the upper limit applies, since the bandwidth of the SQUID is then infinite, whereas the lower limit is valid for a SQUID having $\beta_c = 1$. On the contrary, if β_c is allowed to be much larger than 1, excess noise processes evoked by multiple-mode solutions in the SQUID dynamics tend to increase γ again. Since γ is considered here as a common factor, its value does not affect the optimum substantially. For the equivalent flux noise Φ_n in the SQUID due to the shunt resistor we get, with the help of Eq. (1),

$$\begin{aligned}\Phi_n^2 &= 2\gamma k_B T \left(\frac{L_s^2 (1 - s_f k_s^2)^2}{R} + \frac{R}{G^2} \right) \\ &= \frac{2\gamma k_B T}{R} L_s^2 \left[(1 - k_s^2 s_f)^2 + \left(\frac{2}{g} \right)^2 \left(\frac{1+\beta}{\beta} \right)^2 \right]\end{aligned} \tag{4}$$

Nowadays, the planar technique offers an easy way to improve the magnetic coupling between the input circuit and the SQUID. On the other hand, the desire for low-noise SQUIDs tends to reduce the loop inductance toward the stray inductance set by the fabrication technology. L_{stray} is related to the coupling coefficient k_s^2 by

$$k_s^2 = 1 - L_{\text{stray}} / L_s \tag{5}$$

Here, L_{stray} should be considered to describe the effective stray inductance of the SQUID loop. In other words, all the stray inductance is assumed to be located in the actual SQUID loop. The extrinsic energy sensitivity of the magnetometer can now be given with the aid of Eqs. (2)–(5) as

$$\varepsilon_a = \gamma k_B T \left(\frac{\pi \beta C L_{\text{stray}}}{\beta_c} \right)^{1/2} \frac{(1 - k_s^2 s_f)^2 + (2/g)^2 (1 + 1/\beta)^2}{k_s^2 s_f (1 - s_f)(1 - k_s^2)^{1/2}} \tag{6}$$

The minimum extrinsic energy sensitivity can be readily obtained by varying k_s, s_f, and β. Since g is close to 2, Eq. (6) implies the following choice of

SQUID parameters: $k_s = 0.84$, $\beta = 2.4$, and $s_f = 0.54$. If the damping parameter β_c is not allowed to exceed 0.5, we obtain for the extrinsic energy sensitivity $\varepsilon_a = 100\gamma k_B T(CL_{stray})^{1/2}$ with the optimal choice of parameters. This implies an intrinsic energy sensitivity of the SQUID of $\varepsilon_s = 18\gamma k_B T(CL_{stray})^{1/2}$. Our fabrication technology limits the lowest possible parasitic inductance to 20 pH, and the minimum junction capacitance is 1 pF. Equation (6) predicts that the intrinsic energy sensitivity of our SQUIDs thus cannot be better than 6×10^{-33} J sec. Correspondingly, the minimum theoretically attainable flux noise in a 40-pH SQUID loop is $3 \times 10^{-7}\Phi_0/\sqrt{\text{Hz}}$. As will be discussed in Section 6, these figures were nearly achieved also in practice in our best SQUIDs.

In addition to the estimate of the ultimate sensitivity of the actual magnetometer, the above calculation shows that the SQUID parameters, including the coupling constant, will be determined by the parasitic capacitance and the junction capacitance, which are strongly technology-dependent. In practice, the situation is more complex, but, as will be demonstrated in the following sections, the conclusions will be the same. It should be emphasized that the successful design requires a rather complete elimination of the resonances, and thus many SQUID parameters are restricted. Consequently, only a very successful design may end up with SQUIDs having exactly the predicted characteristics.

3. DESIGN OF THE SQUID

3.1. Selection of the SQUID Geometry

The requirements of low capacitance across the SQUID, high output inductance, and control over the resonances suggest flux coupling via two transformers in series. This approach allows a SQUID of small size, which, in turn, enables one to shift the $\lambda/2$ resonances of the SQUID loop far from the normal operating point. It also turns out that the total length of the flux coupling coil can be allowed to stay long enough to reduce magnetic coupling into the outside world at the average point of operation, simultaneously keeping the capacitance across the SQUID small enough. Consequently, the dynamics of the device will approach that of an autonomous SQUID. This, together with the well-damped input circuits, creates a good basis for the optimization of the SQUID.

The use of an intermediary coupling transformer offers practical advantages, too: the large field-sensing coil can be deposited on a chip different from that on which the actual SQUID, together with the intermediary transformer, is located. This allows flexibility in use: for changing the pickup coil design it is not necessary to alter the SQUID, and inductive coupling

via the transformer eliminates the need for superconducting contacts between the chips.

Since in this structure the SQUID is exposed to the ambient field, particular care has to be exercised to avoid spurious signals caused by homogeneous fields. By constructing the SQUID and the intermediary transformer coils as two-hole configurations, these problems are easily avoided. Such a gradiometric configuration is possible by connecting the loops in parallel or in series.

By coupling the two SQUID loops in parallel, the total inductance is four times smaller than for the series or figure-of-eight configuration. On the other hand, in the series structure the total parasitic capacitance due to the input coil is smaller than for the parallel structure at least by a factor of two, and homogeneous fields do not cause circulating currents as they do in the outer superconducting loop in the parallel structure. In addition, for the series structure it is easier to apply the bias current symmetrically so that it does not couple magnetically to the SQUID.

Since the SQUID noise is proportional to the square root of the total inductance, the parallel configuration is, after all, preferable, since otherwise the SQUID loops would have to be too small. Because of practical linewidth limits, the parasitic inductances will become dominating in miniature structures. Furthermore, the circulating currents should not cause any problems in the SQUID, because of the small loop size resulting from the optimization. This structure is also good for the elimination of transmission line resonances, as discussed in the next section.

In selecting the configuration of the input coil and the intermediate transformer coils the design is mainly dependent on inductance matching. In addition, the possible flux trapping and circulating shielding currents in the structures should be taken more into account, since the intermediary transformer coils are much larger in dimension than the SQUID. Therefore, the figure-of-eight configuration is often preferable over the parallel connection of the loops.

3.2. Elimination of Resonances

As mentioned before, all the resonances caused by the parasitic elements should be pushed to frequencies that have negligible interference with the normal operation of the SQUID. Furthermore, separate damping of resonances is required, since in superconducting structures natural quality factors may be very large.

The SQUID ring, together with the input coil acting as a ground plane, forms a superconducting transmission line activated to resonate when half of the wavelength $\lambda/2$ of the oscillation equals the circumference of the

SQUID loop. The half-wave resonance is strongly coupled to the SQUID dynamics and its frequency may easily be close to the Josephson frequency; it cannot be totally avoided, since proper termination of the transmission line without increasing thermal noise is difficult. Therefore, the dimensions of the SQUID ring should be small enough for shifting the resonance well above the Josephson frequencies at the normal operating points.

The spiral transmission line, formed by the input coil and the SQUID ring as a ground plane, has its fundamental resonance when the total length of the coil on top of the SQUID equals half of the wavelength of the oscillation. In this mode, there are current nodes at the ends of the input coil. There, the stripline leaves the SQUID ring, leading to a sharp rise in the wave impedance of the transmission line. In order to keep this resonance well below the Josephson frequency, the input coil should be made long enough by increasing either the number of turns or the diameter of the SQUID. A compromise must be made, since increased length also increases the capacitance across the SQUID. This first wave resonance is the most important one because coupling to the SQUID weakens with increasing frequency. In our construction, the spiral transmission line resonance is damped by terminating the line with a resistor matched to the stripline impedance. Only one resistor is used, to avoid increased low-frequency thermal noise.

In addition, there may be intrinsic resonances at higher frequencies in which only some portions of the coil take part. They may be damped by placing resistive foil over the input coil. However, to avoid the rise in capacitance across the SQUID and the noise due to thermally induced currents, the foil should be divided into small sections.

In addition to the high-frequency transmission line resonances, the MHz-range *LC* resonance introduced by the flux transformer may be an even more significant source of excess noise. Theoretical and experimental studies have shown that the amount of extra noise generated by the resonant state is proportional to its virtual lifetime, i.e., the Q value divided by the resonance frequency.[12,17] The lifetime can be shortened without introducing thermal noise at the signal frequencies, by connecting a series resistor–capacitor shunt in parallel with the input coil. The damping of the resonance also smoothes the flux-to-voltage characteristics substantially. Although the virtual lifetime and thus the amount of excess noise does not depend directly on the capacitance, the resonance frequency should be high enough to avoid interference with flux modulation carrier frequency and to keep the mixed-down contribution of the resistor noise negligible. The damping shunt also acts as an rf filter whose cutoff frequency should, on the other hand, be low enough to reject interference effectively. However, in the double-transformer structure a second *RC* filter can be connected in parallel with

the pickup coil to filter the input; the shunt nearest to the SQUID thus needs to be optimized only with respect to its resonance damping properties.

3.3. Optimization

As discussed in the previous sections, the use of an intermediary coupling transformer with proper elimination of structural resonances leads to a device whose dynamics can be modeled with the help of an autonomous SQUID. The structure as a whole is mainly dictated by these considerations; optimization merely determines the geometrical dimensions. The avoidance of resonances poses a number of boundary constraints on the minimization of energy sensitivity. Since it is to be expected that the optimum in this multiparameter minimization problem is broad, a detailed expression of the dependence of the energy resolution on the parameters is not needed, nor is the exact value of the minimum. The main point is to have a description of the interrelationships between the parameters.

The equivalent circuit for the optimization is shown in Fig. 1. The sensor is optimized as a single unit, taking into account both the SQUID and the pickup coil. As will be discussed in the following, the best energy resolution, reduced to the pickup coil, depends only on the sensitivity of the SQUID and on the coupling constants of the transformers, provided that these parameters are independent of the pickup loop inductance. Thus, the resulting SQUID is not necessarily tied to one specific pickup coil configuration, but the optimal sensitivity is available for alternative sensing coil designs if the inductances can be matched properly. The constraints

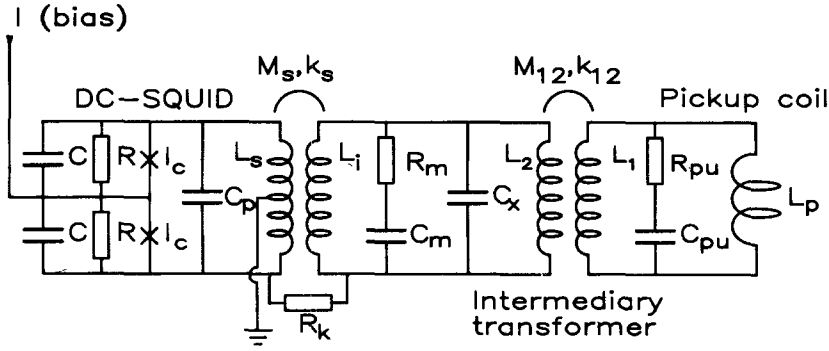

Fig. 1. Equivalent circuit for the complete dc SQUID. Here C_p and C_x denote the parasitic capacitances across the SQUID and over the intermediary transformer, respectively; R_m and C_m are used to damp the resonances in the transformer, and R_{pu} and C_{pu} are employed as an rf shunt. R_k is for terminating the stripline formed by the signal coil. The parasitic inductances are not drawn explicitly, since they can be taken into account in the coupling coefficients between the coils.

on the SQUID are mostly due to the fabrication technology and structural resonances; for determining the structure and the size of the pickup coil one must consider external factors such as the dewar size and the distribution of the magnetic field to be measured.

To calculate the effects of the flux transformers on the SQUID energy sensitivity at signal frequencies, the equivalent circuit of Fig. 1 can be simplified. At low frequencies the capacitances can be ignored, and the circulating current J in the SQUID ring can be taken into account by replacing the input coil inductance L_i by an effective value

$$L_i^{\text{eff}} = L_i(1 - k_s^2 s) \tag{7}$$

where $s = 1 - \Phi_{\text{true}}/\Phi_{\text{applied}}$ is the screening factor of the SQUID due to J. The SQUID, with inductance L_s, can then be considered open-circuited.

Let Φ_n^a be the flux applied to the pickup coil L_p that would transfer to the SQUID a flux equal to the equivalent flux noise Φ_n of the SQUID. Requiring that the flux remains constant inside the superconducting loops, one obtains for the extrinsic energy sensitivity of the double transformer structure

$$\varepsilon_a = \frac{\Phi_n^{a2}}{2L_p} = \frac{[(L_i^{\text{eff}} + L_2)(L_p + L_1) - k_{12}^2 L_1 L_2]^2}{2k_s^2 k_{12}^2 L_i L_1 L_2 L_p L_s} \Phi_n^2 \tag{8}$$

Here, L_1 and L_2 are the inductances of the primary and the secondary of the coupling transformer, respectively, and k_{12} is the coupling between the coils. The coupling coefficient between the SQUID and the input coil L_i is denoted by k_s, Φ_n is the flux sensitivity of the autonomous SQUID, and L_s is the inductance of the SQUID ring. Since generally the coupling coefficients and the intrinsic sensitivity of the SQUID depend on the inductances in the intermediary transformer in a complex way, Eq. (8) cannot be minimized analytically. However, to gain some insight into signal losses introduced by the flux transformer, it is instructive to estimate the optimum transformer design by assuming the coupling coefficients and the SQUID sensitivity to be constant. Then, the minimum energy sensitivity of the whole sensor is

$$\varepsilon_a = \frac{4[1 + (1 - k_{12}^2)^{1/2}]^2}{k_s^2 k_{12}^2} (1 - k_s^2 s) \frac{\Phi_n^2}{2L_s} \tag{9}$$

provided that the inductances of the intermediary coil satisfy

$$L_1 = \frac{L_p}{(1 - k_{12}^2)^{1/2}} \tag{10}$$

$$L_2 = \frac{L_i^{\text{eff}}}{(1-k_{12}^2)^{1/2}} \tag{11}$$

In the following, it will be shown that the intrinsic sensitivity of the SQUID does not depend on the actual values of L_p, L_1, L_2, and L_i^{eff}, but on their ratios L_1/L_p and L_2/L_i^{eff}. Thus, in this first-order approximation, the minimum energy resolution of the whole sensor is a function of the SQUID sensitivity and the coupling coefficients only. Note that in optimum, the pickup and the input coils are matched to the effective inductances of the primary and the secondary of the intermediary transformer, respectively.

To calculate the intrinsic energy sensitivity of the SQUID we used similar methods as described by Tesche in analyzing her double-loop SQUID.[8] Since the length of the input coil is assumed to be long compared with the wavelength of the Josephson oscillations, the inductance of the SQUID loop sensed by the high-frequency dynamics remains the same as the geometric inductance. On the other hand, the dc inductance is screened by the coupling circuit. Consequently, we may write for the inductance

$$L_{\text{dc}} = (1-k_s^2 s_{\text{in}})L_s \tag{12}$$

sensed by low-frequency circulating currents. Here,

$$s_{\text{in}} = \frac{(L_p+L_1)L_i}{(L_p+L_1)(L_2+L_i)-k_{12}^2 L_1 L_2} \tag{13}$$

is the screening factor due to the input circuits.

When the SQUID dynamics is assumed to be free from multiple modes and resonances caused by the flux coupling circuits, the flux transformer coils affect the intrinsic energy sensitivity of the SQUID only via s_{in}, which depends only on the inductance ratios L_1/L_p and L_2/L_i, provided, of course, that the coupling coefficients are kept constant.

Solving the dc SQUID differential equations, including all the input circuit effects, requires massive numerical simulations. On the other hand, the dynamics of the autonomous SQUID has been studied extensively by numerical and analog simulations.[21,22,24] The solutions of an autonomous SQUID can be used to derive the corresponding characteristics of the whole SQUID, provided that the parasitic elements do not perturb the SQUID dynamics. Approximate analytical expressions, derived on the basis of the numerical simulations, are used for calculating the forward transfer gain and the circulating current of the dc SQUID.

The equivalent flux noise of the SQUID can be obtained from Eq. (4), with slight modifications caused by the screening current in the SQUID loop. Again, the indirect contribution of the shunt resistors is taken into

account by the factor γ. Therefore, we find, as in Eq. (4),

$$\Phi_n^2 = 2\gamma k_B T \left(\frac{R}{G^2} + \frac{L_{dc}^2}{R} \right) \tag{14}$$

The forward flux-to-voltage transfer function $G = \partial V / \partial \Phi_s^a$ is calculated with respect to the flux Φ_s^a applied to the SQUID. However, the response to a magnetic flux is determined as if the input flux Φ_s^{in}, sensed by the ac dynamics of the SQUID, i.e., by an equivalent autonomous SQUID with inductance parameter β, were modified to

$$\Phi_s^{in} = \Phi_s^a + s_{in} k_s^2 L_s J \tag{15}$$

where J is the low-frequency circulating current in the SQUID loop. For the circulating current, we used the approximation

$$J = -\left(\frac{1}{3+\beta} \frac{\Phi_s^{in}}{\Phi_0} - \frac{1}{2} \right) I_0 \tag{16}$$

where $\beta = 2L_s I_0 / \Phi_0$. This linearization is accurate only in the input flux region around $\Phi_s^{in} = \Phi_0/2$. It still holds, however, reasonably well at the normal flux bias points $\Phi_s^{in} = \Phi_0/4$ and $\Phi_s^{in} = 3\Phi_0/4$ used in the usual flux modulation scheme.

The use of the rather crude approximation for J can be justified by two arguments. First, at $\beta \simeq 1$, which is known to be the optimum for an autonomous SQUID, the match to the numerically simulated values at ordinary current and flux bias working points[21] is good. Second, the effect of the circulating current is fairly low and smoothly varying near the minimum of the energy sensitivity in the parameter space.

The forward transfer function G of the SQUID can be be approximated by

$$G = \frac{\partial V}{\partial \Phi_s^a} = \frac{\partial V}{\partial \Phi_s^{in}} \frac{\partial \Phi_s^{in}}{\partial \Phi_s^a} \tag{17}$$

Since Φ_s^{in} and Φ_s^a are coupled together via the circulating current J through Eqs. (15) and (16), we may write

$$G \simeq \frac{g}{(1+\beta)(1+\beta_c+2\beta_k)^{1/2}} \frac{2(3+\beta)}{2(3+\beta)+\beta s_{in} k_s^2} \frac{I_0 R}{\Phi_0} \tag{18}$$

The first factor in Eq. (18) is the transfer function of the autonomous SQUID; see Eq. (1). It is modified to include the effects of the junction capacitance C and the parasitic capacitance C_p across the SQUID (see Fig. 1) by the parameters $\beta_c = 2\pi I_0 R^2 C / \Phi_0$ and $\beta_k = 2\pi I_0 R^2 C_p / \Phi_0$, respectively.

Inserting Eq. (18) into (14), we get finally the equivalent flux noise of the SQUID,

$$\Phi_n^2 = 2\gamma k_B T L_s (L_s C)^{1/2} \left(\frac{\pi\beta}{\beta_c}\right)^{1/2} \times \left\{ \frac{(1+\beta)^2(1+\beta_c+2\beta_k)[2(3+\beta)+s_{in}k_s^2\beta]^2}{\beta^2 g^2(3+\beta)^2} + (1-k_s^2 s_{in})^2 \right\} \quad (19)$$

The energy resolution of the complete sensor, Eq. (8) together with Eq. (19), is complicated to minimize analytically, so a suitable multivariable minimization algorithm for nonlinear functions was used.[25] In the minimization, the coupling coefficients cannot be assumed to be constant; the dependence on the geometry must be taken into account. Thus, the straightforward minimization described in Section 2.2 does not strictly apply. As a result, the parameters in the optimum will differ somewhat from those predicted by that idealized analysis.

To take into account the practical limitations of fabrication, the SQUID and the coil parameters were expressed as functions of actual geometrical dimensions, which were then employed in the optimization. This allows the use of constraints relevant in the fabrication technology, such as the minimum allowed linewidth, feasible film thicknesses, maximum resistivities of the resistor foils, and permittivities of the insulators. Some of the approximate analytical formulas to calculate the various inductances and coupling

TABLE I

SQUID and Flux Transformer Parameters (Nominal)

SQUID inductance	$L_s = 80$ pH
Junction critical current	$I_0 = 50\ \mu$A
Junction shunt resistance	$R = 1.0\ \Omega$
Junction capacitance	$C = 1$ pF
Junction area	$A = 2.5 \times 2.5\ \mu m^2$
Stewart-McCumber parameter	$\beta_c = 0.3$
Parasitic capacitance parameter	$\beta_k = 0.1$
Screened inductance parameter	$\beta_{dc} = 1.0$
$\lambda/2$ resonance of the SQUID	$f_s = 150$ GHz
$\lambda/2$ resonance of the input coil	$f_i = 5$ GHz
Input coil inductance	$L_i = 34$ nH
Coupling between SQUID and input coil	$k_s = 0.9$
Number of turns in input coil	$n_i = 10$
Transformer secondary inductance	$L_2 = 25$ nH
Number of turns in the transformer secondary	$n_2 = 2$
Screening factor, with the pickup coil chip	$s_{in} = 0.7$
Intermediate transformer shunt resistance	$R_m = 4\ \Omega$
Intermediate transformer shunt capacitance	$C_m = 300$ pF
Resonance frequency of the intermediate transformer	$f_{res} = 130$ MHz
Q value of the intermediate transformer	$Q = 1.5$

coefficients are listed in the Appendix. The pickup coil and the intermediary transformer primary were designed to be used in a multichannel first-order planar gradiometer for neuromagnetic research.[26]

Because it was inconvenient to incorporate all practical design considerations into the model that we employed in the minimization process, some of the parameters obtained by the straightforward computation were finally fine-tuned manually. This was to secure reliable and stable operation of the SQUID and to increase its tolerance to parameter variations, especially against lower coupling coefficients than the calculated ones. These modifications included lowering the β and β_c by altering the critical current and resistance values and increasing the number of turns in the input coil from nine to ten to keep the input coil $\lambda/2$ resonance well below the Josephson frequency at the normal point of operation. The resulting parameters of the SQUID and the flux transformer coils located on the SQUID chip are summarized in Table 1. With these component values, Eq. (19) predicts an intrinsic flux noise $\Phi_n = 1.0 \times 10^{-6} \Phi_0 / \sqrt{\text{Hz}}$. In this estimate, $\gamma = 2$ was used, since our SQUID is well-damped, increasing the contribution of the mixed-down noise. In order to damp properly the parasitic capacitance $C_x \simeq 70$ pF across the intermediate transformer, a shunt with $R_m = 4\Omega$ and $C_m = 300$ pF was chosen. This implies a $Q \simeq 1.5$ and a resonant frequency of about 130 MHz. With these component values the excess noise due to the resonance is eliminated; in addition, the noise contribution of the shunt resistor at signal frequencies and at the Josephson frequency is negligibly small.

4. STRUCTURE AND FABRICATION OF THE SQUID

Based on this design and optimization, a dc SQUID with an intermediary transformer was fabricated. In addition, a separate gradiometer pickup coil chip[26] was made.

The realization of the SQUID structure discussed here requires a total of ten mask layers. The whole SQUID chip, size 6×9 mm^2, is shown in Fig. 2a. The secondary coils of the intermediary transformer occupy most of the area of the figure; the coils, connected in series, have two turns with an inner diameter of 2 mm and an outer diameter of 4 mm. In the bottom are the contact pads for bias current, voltage measurement, and flux modulation. The flux modulation coil is coupled inductively to the secondary of the intermediary transformer. The actual dc SQUID is located on top of the figure, in the middle; a closeup is shown in Fig. 2b. The SQUID loops, with an inner diameter of 100 μm and an outer diameter of 260 μm, are connected in parallel, and the window-type Josephson junctions, size 2.5×2.5 μm^2, are in the center of the structure. Bias current and voltage measure-

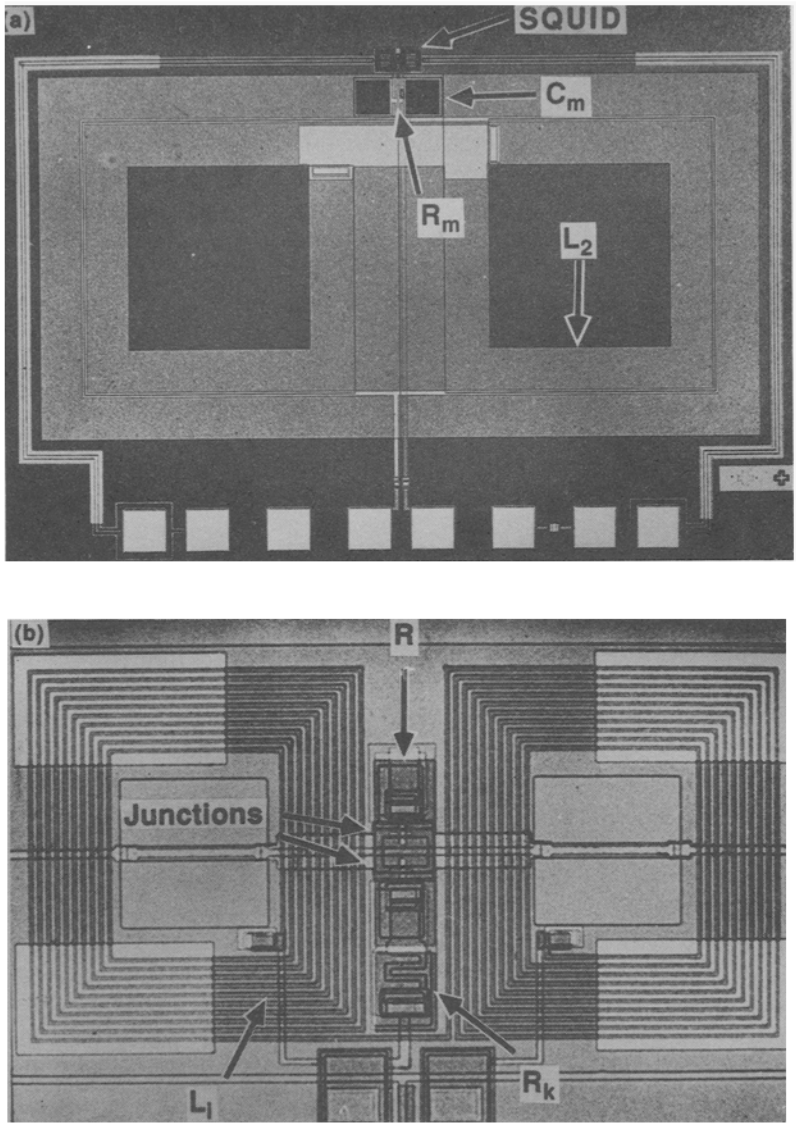

Fig. 2. (a) Photograph of the complete dc SQUID chip, of size 6×9 mm^2. The SQUID itself is on top of the structure, in the middle; most of the area of the figure is occupied by the secondary of the intermediate transformer (L_2). The primary and the pickup coil are on a separate chip, which is placed on top of the SQUID chip. At the bottom, contact pads for bias current, flux modulation, and signal measurement are seen; the shunt R_mC_m used for damping the input coil resonances is below the SQUID. (b) Closeup of the dc SQUID. The Josephson junctions are in the center of the figure, and the bias is applied symmetrically from the sides. The junction shunt resistors R are seen above and below the junctions. Below the lower shunt resistor is the terminating resistor R_k of the input coil. The edge of the SQUID hole is 100 μm.

ment leads are fed symmetrically from the side over the SQUID hole to prevent magnetic coupling. The shunt resistors are above and below the Josephson junctions; below the lower shunt is the terminating resistor for the input coil strip transmission line. The input coil has two coils of ten turns connected in series. The width of the conductors is 3 μm, and the separation between the strips is 3 μm. A series coupling of two capacitors and a resistor, located just below the SQUID, is connected across the input coil to damp the resonances in the MHz range. In addition, insulated resistive foils are placed on top of the input coil to damp possible higher resonance modes.

The SQUID loop and the intermediary transformer secondary coil are dc magnetron sputtered of Nb target on an oxidized silicon substrate and patterned with reactive ion etching. The capacitors for the input coil shunt are formed by anodizing the Nb base electrode[27] before the Nb film patterning and by depositing a Cr/Au counterelectrode, to be covered later by a Pb film and connected to a resistor. The capacitors, 0.6 nF each, occupy an area of 360×360 μm^2. Next, two 180-nm-thick insulating layers of silicon oxide are electron-gun evaporated on top of Nb, with cross windows for Josephson junctions and rectangular windows for contacts. The SiO layer is deposited in two stages using two different masks to avoid short-circuits caused by pinhole defects.

The Josephson junctions are formed by dc plasma discharge oxidation in a premixed 95% Ar/5% O_2 atmosphere at a pressure of 3 Pa. Before the oxidation, the native oxides are removed by 15 min of 500-eV ion beam etching with a current density of 0.17 mA/cm^2, followed by 5 min at 200 eV and 0.51 mA/cm^2 to reduce the ion bombardment damage to the Nb surface. During this preclean process the substrates heat above 60°C; uncontrolled thermal oxides will thus form from the process gases during the initial stages of the plasma discharge preparation. The samples are therefore allowed to cool down to the ambient temperature in a vacuum better than 30 μPa, and, immediately before the plasma process, the substrates are etched for 2 min with an 200-eV ion beam with a current density of 0.51 mA/cm^2. Typically, the samples are plasma-oxidized 39–41 sec at a discharge voltage of 1.6 kV and a current of 9 mA.

The counterelectrodes for the Josephson junctions are electron-gun-evaporated from a 87.5 w% Pb/12.5 w% In alloy source to a thickness of 250 nm, followed by a 10 nm layer of SiO for process passivation. The shunt resistors of the junctions and of the input coil shunt are then deposited by evaporating 200 nm of Ti followed by 20 nm of Au, giving a square resistance of 1 Ω. The SQUID is insulated from the 500-nm thick Pb–In input coil by a 750-nm-thick double layer of SiO. The second Pb layer also forms the flux modulation coil. All the crossovers necessary for the coils are made

with the help of the first deposited Pb layer. Finally, the whole chip is passivated with 700 nm of SiO. The films are patterned using liftoff photolithography, except for the reactive-ion-etched base electrode and the second lead-alloy film, which is ion-beam-etched.

5. SQUID ELECTRONICS

The block diagram of the SQUID electronics is illustrated in Fig. 3. The low output impedance of the SQUID, 2–5 Ω, is stepped up to a few kilo-ohms by means of a cooled transformer. To minimize the effective output capacitance and, correspondingly, to maximize the bandwidth of the transformer, the number of turns in the transformer should be chosen so that its self-resonance is at the operation frequency. The higher the bandwidth of the transformer, the higher the maximum slew rate that can be realized. If a lower bandwidth is sufficient, the resonance frequency can also be set by the use of an external capacitor.

The first stage of the amplifier chain consists of two low-noise junction field effect transistors (Toshiba SK 146) coupled in parallel. The current noise with the preamplifier at 100 kHz was measured to be 100 fA/$\sqrt{\text{Hz}}$ and the voltage noise 0.4 nV/$\sqrt{\text{Hz}}$. These figures imply a noise temperature of 2 K and an optimal input impedance of 4 kΩ. Since the effective noise temperature of the SQUID is more than 20 K, the noise contribution of the preamplifier remains negligibly small. The drain current of the FETs is stabilized by injecting the control voltage to the gates of the transistors through a feedback resistor. The value of the resistance is small enough to damp slightly the resonating input circuit, but high enough not to increase

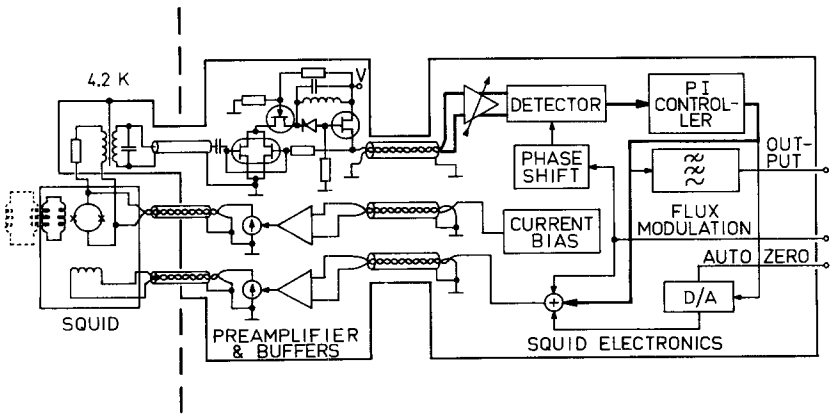

Fig. 3. A schematic diagram of the electronics. See text for details.

the noise temperature of the preamplifier. The damping via a negative feedback increases the frequency bandwidth and thus the slew rate of the system. The bandwidth of the first amplifier stage with the transformer is 10 kHz. The preamplifier unit also contains buffers for the bias current and flux modulation and feedback. Therefore, possible variations in the line impedance caused by temperature fluctuations do not affect the signals.

The SQUID is operated using square-wave flux modulation. Correspondingly, the amplified signal is detected phase-sensitively by the demodulator circuit. It is common that the demodulator consists of a mixer and a low-pass postdetection filter. In our configuration, however, the signal is multiplied by the modulation and it is then integrated over a half period of the modulation frequency. After that, the signal is fed into a sample-and-hold circuit. Consequently, the modulation signal and its harmonics are effectively rejected. This approach allows a much higher feedback gain, and thus a higher slew rate, than in a device with a conventional detection scheme.

The electronics is equipped with circuits allowing remote control. Also, an external flux modulation signal can be used in order to run several SQUID systems simultaneously. The feedback may be routed via the D/A converter to automatically set the output of the SQUID to zero, which is useful in recovery after flux trapping.

6. EXPERIMENTAL RESULTS

Each SQUID chip also contains unshunted test junctions for evaluation of the critical current spread and the junction barrier quality. As a figure-of-merit, the V_m parameter, defined as the critical current times the resistance at 2 mV, is used.[28] An example of the measured current–voltage characteristics for a $3 \times 3\ \mu m^2$ test junction is shown in Fig. 4. Typically, the V_m parameter is around 20 mV, indicating good quality, i.e., low-leakage junction barriers.

The characteristics of the SQUID were measured both with and without the pickup coil connected to the secondary of the intermediate transformer. An example of the current–voltage curves is shown in Fig. 5, recorded for two flux values. The apparent inductance of the SQUID with the input coil and the secondary of the transformer is 40 pH. Using the calculated inductance of the SQUID ring, 80 pH, this gives a coupling coefficient $k_s = 0.9$ between the SQUID and the input coil, in good agreement with the theoretically predicted value of k_s. The pickup coil of inductance 170 nH and the intermediary transformer primary coil of inductance 570 nH reduce the apparent SQUID inductance to 30 pH, which indicates a coupling coefficient $k_{12} = 0.8$ in the transformer.

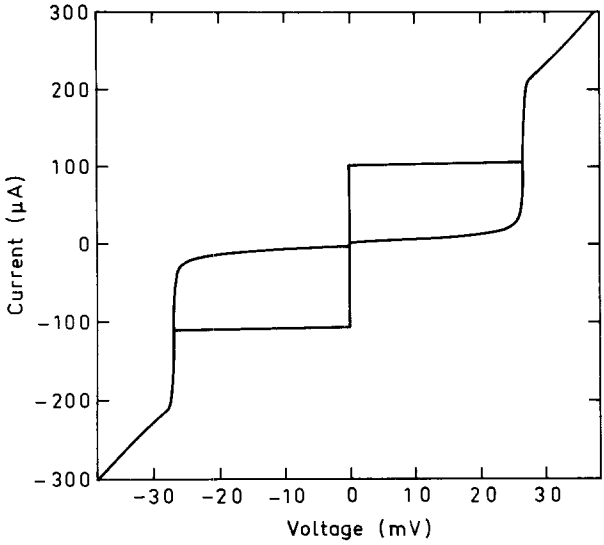

Fig. 4. Current-voltage characteristics of a $3 \times 3\ \mu m^2$ unshunted test junction. The V_m parameter is 18 mV, and the normal-state tunneling resistance 11 Ω.

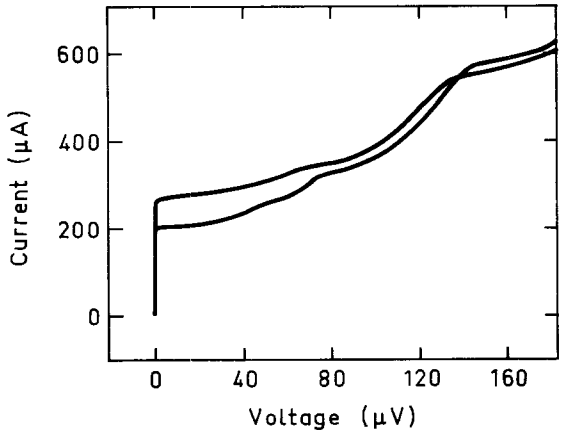

Fig. 5. Current-voltage characteristics of one of our SQUIDs, connected to a pickup coil chip. Note the beat resonance at 140 μV. At 80 μV a partially damped resonance is seen whose origin is unknown, however, since this resonance is well above the normal operating point, it does not cause any problems.

The flux-to-voltage characteristics of the SQUID show a smooth behavior with no extra resonances at bias levels where the gain is at maximum, as shown in Fig. 6. The voltage plateau at 140 μV indicates the beat resonance of the SQUID ring, in agreement with the calculated value.

The noise measurements were carried out in a complete practical experimental setup, i.e., the SQUID connected via a resonant transformer to the preamplifier and detector/controller unit, which operated the SQUID in a flux-locked loop with the usual square-wave flux modulation scheme. Noise levels were measured both with and without a gradiometer pickup coil connected to the SQUID. In both cases, the SQUID and the optimal gradiometer were kept inside a superconducting shield and the measurements were performed in our magnetically shielded room[29] to remove environmental noise. The noise voltages were measured with a HP 3561A FFT signal analyzer using Hanning windowing, and the traces were calibrated to read flux units by separately determining the change in output voltage corresponding one flux quantum change in the flux threading the SQUID ring.

The white noise level of our SQUIDs is below $5\times10^{-6}\,\Phi_0/\sqrt{\text{Hz}}$, corresponding to an $\varepsilon_s < 6\times10^{-31}$ J sec, and the lowest measured noise, with the input coil connected, was $1.3\times10^{-6}\,\Phi_0/\sqrt{\text{Hz}}$, corresponding to $\varepsilon_s = 4\times10^{-32}$ J sec. An example of the measured noise spectra is shown in Fig. 7. The low-frequency noise corner point is around a few Hz. Due to the relatively low $1/f$ noise, no special current modulation schemes were required. The performance of our SQUIDs is thus comparable to or better

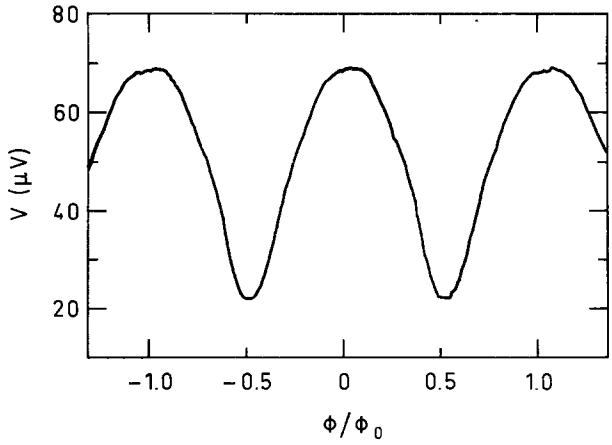

Fig. 6. The flux-to-voltage characteristic of the SQUID shown in Fig. 5, recorded at 255 μA, where the gain is at maximum.

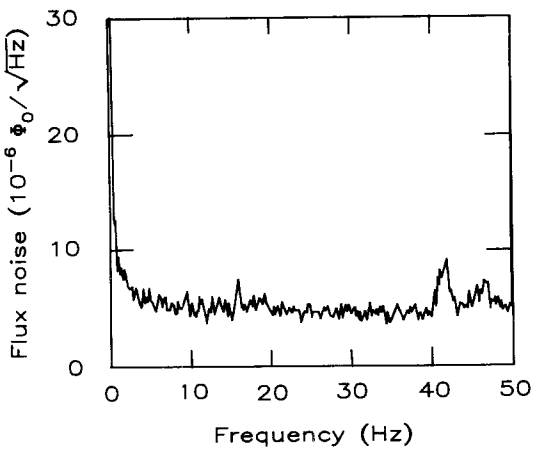

Fig. 7. An example of noise spectra, measured from the SQUID shown in Figs. 5 and 6, recorded at maximum gain bias. A flux-locked loop with conventional flux modulation was used. The extra peak above 40 Hz is due to a mechanical resonance.

than that of other *practical* SQUID sensors; however, the yield of the fabrication process is small, so far.

7. DISCUSSION

The problems associated with the design of tighly coupled, low-noise dc SQUID magnetometers have been discussed. The key points of the design were the elimination of the parasitic capacitance, the *LC* resonances, and the transmission line resonances, all due to the signal coil. This is necessary for obtaining smooth characteristics, which form a solid foundation for the optimization of the sensitivity, justified by a dc SQUID designed and produced by following these design principles. The lowest flux noise, measured in a practical setup with flux-locked loop, was comparable to calculations where only the thermal noise from the shunt resistors was included. These results imply that the SQUIDs do not suffer from excess noise sources introduced by multiple modes in the SQUID dynamics. The lowest available flux noise was, however, four times that predicted by an idealized model where the junction capacitance and the stray inductance were assumed to be the only limitations. That seems to indicate that a slight enhancement in sensitivity could be gained. Further improvement could be attained by increasing β_c, accomplished by raising the values of the shunt resistors. In addition, higher β_c lowers the bandwidth, diminishing the

contribution of mixed-down noise. However, the reduction of damping would eventually disturb the smooth characteristics and invite multiple modes, with well-known consequences.

The main objective of this project was to develop practical SQUIDs for multichannel applications; the realization of a reliable and easy-to-use SQUID sensor with sufficiently low noise was more important than aiming at the highest possible energy sensitivity. These requirements were fulfilled in the developed dc SQUID; no further improvements of the SQUID design are necessary. Only a radical change in the fabrication technology would put the design against new challenges.

APPENDIX

This appendix lists some of the approximate analytical formulas used to calculate inductances and coupling coefficients.

1. Square washer, hole diameter d, edge width w,[30,31]

$$L = 1.25\,\mu_0 d; \qquad d \le w \tag{A1}$$

$$L = \frac{2}{\pi}\mu_0 l\left(\ln\frac{l}{w} + \frac{1}{2}\right); \qquad d > w \tag{A2}$$

2. Stripline of width w and of length l, a distance of h over a ground plane[32]:

$$L = \mu_0 \frac{lh}{w}\frac{1}{K_f(w, h, t)} \tag{A3}$$

where $K_f(w, h, t)$ is the fringe field factor (see ref. 32) and t is the stripline film thickness.

3. Coplanar strip transmission line of length l, conductors of width w separated by d,[33,34]

$$L = \mu_0 l \frac{K(k)}{K([1-k^2]^{1/2})} \tag{A4}$$

where $K(k)$ is the complete elliptic integral of the first kind and $k = d/(d+w)$.

4. Planar transformer with turns ratio $1:n$,[35]

$$L_{\text{secondary}} = n^2(L_{\text{primary}} - L_{\text{par}}) + L_{\text{strip}} \tag{A5}$$

and coupling coefficient

$$k^2 = \left(1 + \frac{L_{\text{strip}}}{n^2(L_{\text{primary}} - L_{\text{par}})}\right)^{-1}\left(1 - \frac{L_{\text{par}}}{L_{\text{primary}}}\right) \tag{A6}$$

where L_{strip} is the stripline inductance of the secondary over the transformer primary and L_{par} is the parasitic inductance associated with the transformer primary.

ACKNOWLEDGMENTS

The authors thank Dr. Antti Ahonen, Prof. Juhani Kurkijärvi, and Tapani Ryhänen for valuable discussions during the work, Istvan Derka and Jari Hällström for the construction of the SQUID electronics, and Prof. Olli V. Lounasmaa for comments on the manuscript.

This work was supported by SITRA, TEKES, and by the Academy of Finland.

REFERENCES

1. J. Clarke, *Physica* **126B**, 441 (1984).
2. C. D. Tesche, K. H. Brown, A. C. Callegari, M. M. Chen, J. H. Greiner, H. C. Jones, M. B. Ketchen, K. K. Kim, A. W. Kleinsasser, H. A. Notarys, G. Proto, R. H. Wang, and T. Yogi, *IEEE Trans. Magn.* **MAG-21**, 1032 (1985).
3. C. M. Pegrum, D. Hutson, G. B. Donaldson, and A. Tugwell, *IEEE Trans. Magn.* **MAG-21** 1036 (1985).
4. T. Noguchi, N. Ohkawa, and K. Hamanaka, in *SQUID'85, Superconducting Quantum Interference Devices and Their Applications*, H. D. Hahlbohm and H. Lübbig, eds. (Walter de Gruyter, Berlin, 1985), p. 761.
5. B. Muhlfelder, J. A. Beall, M. W. Cromar, and R. H. Ono, *Appl. Phys. Lett.* **49**, 1118 (1986).
6. M. Nakanishi, M. Koyanagi, S. Kosaka, A. Shoji, M. Ayoagi, F. Shinoki, H. Nakagawa, S. Takada, N. Kasai, H. Kado, and T. Endo, in *Extended Abstracts of the* 1987 *International Superconductivity Electronics Conference ISEC'87* (Japan Society of Applied Physics, Tokyo, 1987), p. 265.
7. Y. Katoh, H. Asano, K. Tanabe, and O. Michikami, in *Extended Abstracts of the* 1987 *International Superconductivity Electronics Conference ISEC'87* (Japan Society of Applied Physics, Tokyo, 1987), p. 277.
8. C. D. Tesche, *J. Low Temp. Phys.* **47**, 385 (1982).
9. M. Gershenson, R. Hastings, R. Schneider, M. Sweeny, and E. Sorensen, *IEEE Trans. Magn.* **MAG-19**, 2058 (1983).
10. K. Enpuku, K. Sueoka, K. Yoshida, and F. Irie, *J. Appl. Phys.* **57**, 1691 (1985).
11. D. Drung and W. Jutzi, in *SQUID'85, Superconducting Quantum Interference Devices and Their Applications*, H. D. Hahlbohm and H. Lübbig, eds. (Walter de Gruyter, Berlin, 1985), p. 807.
12. H. Seppä and T. Ryhänen, *IEEE Trans. Magn.* **MAG-23**, 1083 (1987).
13. C. Hilbert and J. Clarke, *J. Low Temp. Phys.* **61**, 237 (1985).
14. P. Carelli and V. Foglietti, *IEEE Trans. Magn.* **MAG-19**, 299 (1983).
15. P. Carelli and V. Foglietti, *IEEE Trans. Magn.* **MAG-21**, 424 (1985).
16. B. Muhlfelder, J. A. Beall, M. W. Cromar, R H. Ono, and W. W. Johnson, *IEEE Trans. Magn.* **MAG-21**, 427 (1985).
17. J. Knuutila, A. Ahonen, and C. Tesche, *J. Low Temp. Phys.* **68**, 269 (1987).
18. K. Enpuku, T. Muta, K Yoshida, and F. Irie, *J. Appl. Phys.* **58**, 1916 (1985).
19. K. Enpuku and K. Yoshida, *J. Appl. Phys.* **59**, 1714 (1986).
20. K. Enpuku, K. Yoshida, and S. Kohjiro, *J. Appl. Phys.* **60**, 4218 (1986).
21. C. D. Tesche and J. Clarke, *J. Low Temp. Phys.* **29**, 301 (1977).
22. V. J. de Waal, P. Schrijner, and R. Llurba, *J. Low Temp. Phys.* **54**, 215 (1984).

23. V. J. de Waal, T. M. Klapwijk, and P. van den Hamer, *J. Low Temp. Phys.* **53**, 287 (1983).
24. J. A. Ketoja, J. Kurkijärvi, T. Ryhänen, and H. Seppä, *Phys. Rev. B* **35**, 404 (1987).
25. D. Himmelblau, *Applied Nonlinear Programming* (McGraw-Hill, New York, 1972).
26. J. Knuutila, M. Kajola, R. Mutikainen, and J. Salmi, in *Extended Abstracts of the* 1987 *International Superconductivity Electronics Conference ISEC*'87 (Japan Society of Applied Physics, Tokyo, 1987), p. 261.
27. R. E. Joynson, C. A. Neugebauer, and J. R. Rairden, *J. Vac. Sci. Technol.* **4**, 171 (1967).
28. R. F. Broom, S. I. Raider, A. Oosenbrug, R. E. Drake, and W. Walter, *IEEE Trans. Electron Dev.* **ED-27**, 1998 (1980).
29. V. O. Kelhä, J. M. Pukki, R. S. Peltonen, A. A. Penttinen, R J. Ilmoniemi, and J. J. Heino, *IEEE Trans. Magn.* **MAG-18**, 260 (1982).
30. J. M Jaycox and M. B. Ketchen, *IEEE Trans. Magn.* **MAG-17**, 400 (1981).
31. M. B. Ketchen, *J Appl. Phys.* **58**, 4322 (1985).
32. W. H. Chang, *J. Appl Phys.* **50**, 8129 (1979).
33. W. H. Chang, *J. Appl. Phys.* **52**, 1417 (1981).
34. C. P. Wen, *IEEE Trans. Microwave Theory Techn.* **MTT-17**, 1087 (1969).
35. M. B. Ketchen, *IEEE Trans. Magn.* **MAG-17**, 387 (1981).